http://dx.doi.org/10.5516/NET.02.2014.023

RECENT IMPROVEMENTS IN THE CUPID CODE FOR A MULTI-DIMENSIONAL TWO-PHASE FLOW ANALYSIS OF NUCLEAR REACTOR COMPONENTS

HAN YOUNG YOON[1*], JAE RYONG LEE[1], HYUNGRAE KIM[1], IK KYU PARK[1], CHUL-HWA SONG[1], HYOUNG KYU CHO[2], and JAE JUN JEONG[3]
[1]Korea Atomic Energy Research Institute, 989-111 Daeduk-daero, Daejeon, 305-353 Korea
[2]Department of Nuclear Engineering, Seoul National University, Seoul, 151-742, Korea
[3]School of Mechanical Engineering, Pusan National University, Busan, 609-735, Korea
[*]Corresponding author. E-mail : hyyoon@kaeri.re.kr

Received February 28, 2014
Accepted for Publication July 09, 2014

The CUPID code has been developed at KAERI for a transient, three-dimensional analysis of a two-phase flow in light water nuclear reactor components. It can provide both a component-scale and a CFD-scale simulation by using a porous media or an open media model for a two-phase flow. In this paper, recent advances in the CUPID code are presented in three sections. First, the domain decomposition parallel method implemented in the CUPID code is described with the parallel efficiency test for multiple processors. Then, the coupling of CUPID-MARS via heat structure is introduced, where CUPID has been coupled with a system-scale thermal-hydraulics code, MARS, through the heat structure. The coupled code has been applied to a multi-scale thermal-hydraulic analysis of a pool mixing test. Finally, CUPID-SG is developed for analyzing two-phase flows in PWR steam generators. Physical models and validation results of CUPID-SG are discussed.

KEYWORDS : The CUPID Code, Domain Decomposition Parallel Method, Code Coupling Via Heat Structure, Steam Generator

1. INTRODUCTION

Over the past several decades, system thermal-hydraulic codes, such as MARS [1], RELAP [2] and CATHARE [3], have been widely used to support the licensing procedure for nuclear reactors. Some of these codes, even though they are based on a one-dimensional approach, have provided new modeling capabilities for more realistic calculations. However, more advanced three-dimensional two-phase flow modeling is required for the safety assessment of advanced nuclear reactors, especially for new reactors equipped with passive safety systems. Recently, CMFD (Computational Multi Fluid Dynamics) codes are able to predict the multi-dimensional two-phase flow of a nuclear reactor, in part with the advancement of high performance computers. For instance, a pressurized thermal shock phenomenon, which is one of the important safety issues of PWRs, has been successfully analyzed using the NEPTUNE_CFD code [4].

KAERI has been developing a CMFD code named CUPID [5,6] for the analysis of transient two-phase flows in nuclear reactors, based on a transient two-fluid, three-field model. The two fluids are gas and liquid, and the three fields refer to gas, continuous liquid and droplets. Relevant physical models have been developed to close the governing equations, such as interfacial transfer models and the equations of state. The governing equations are integrated and discretized using the finite volume method over unstructured meshes. In the numerical method of CUPID, all the primary variables are defined at cell center. Discretized linear equations are solved using a semi-implicit numerical method, which is more efficient in analyzing a transient two-phase flow than a SIMPLE-based implicit method [7]. The CUPID code has been validated against a set of test problems consisting of conceptual problems and experimental data [8, 9].

In this paper, recent advances in the CUPID code are presented. The key features include the parallelization of CUPID, the coupling with a system analysis code via heat structure, and the development of the CUPID-SG code to apply to the thermal-hydraulic analysis of pressurized water reactor (PWR) steam generators.

A large number of computing cells are required for the simulation using a CMFD code, which leads to a huge

computational load. To overcome this problem, the parallel computing comes with higher priority. Parallel computing using OpenMP library [10] had been implemented in the previous version of CUPID and used for a multi-core processor PC (Personal Computer). The maximum speedup is limited to the number of cores (i.e., 4 for a quad-core PC) since it is based on a shared memory system. A domain decomposition parallel computing scheme is implemented in the present version of CUPID for application to a cluster computer, which consists of multiple processors and memories. All the global variables are partitioned for each processor and the data communication among processors is achieved using the MPI (Message Passing Interface) library [11]. The domain decomposition method for the pressure matrix solver of CUPID is described in detail. Then the parallel performance is discussed for a conceptual problem with respect to the number of processors up to 50.

In a multi-scale thermal-hydraulics analysis, the behavior of an entire nuclear reactor system is simulated by using a system-scale code while local phenomena are addressed using a meso-scale (CFD- or component-scale) code. Direct coupling of a meso-scale code with a system-scale code is one of the best practices to realize the multi-scale analysis. In the previous study [12], the meso-scale code CUPID had been coupled with the system-scale code, MARS, where the pressure matrices of both codes were integrated to solve the flow field simultaneously. In the present study, the CUPID code is coupled again with the MARS code via the heat structure of MARS. There is no fluid flow exchange through the heat structure. In this method, the flow fields of both codes need not to be calculated at the same time, and thus the numerical implementation is rather simple. For the verification of the heat structure coupling, the pool mixing test [13], which is a performance validation experiment for the PAFS (Passive Auxiliary Feedwater System) of APR+, is simulated. The long transient, which lasted for about 8 hours, was successfully analyzed using the coupled code and the results are discussed.

The CUPID code has been developed to apply to the two-phase flow analysis for nuclear reactors in CFD or component scales. In a component scale analysis, a porous medium model is usually applied, since the computing cell is too large to describe the internal structure. The component scale calculation is very useful for the safety and performance analysis of reactor components, such as PWR steam generators. CUPID-SG has been developed as a practical application of CUPID in component scale for analyzing two-phase flows and heat transfer in PWR steam generators. A porous media model is applied for the complex internal structures in a steam generator shell, including the U-tube bundle. The two-phase flow regime, interfacial heat and momentum transfer models, and wall friction models employed in CUPID-SG are introduced. It is validated against the FRIGG test and the results are discussed, together with those of the ATHOS code [14].

2. PARALLELIZATION OF THE CUPID CODE

A component- or CFD-scale analysis related to nuclear thermal-hydraulic issues usually involves a huge number of computational meshes. For instance, the CFD-scale simulation of fluid flow in a single fuel assembly of a reactor core requires about 10^8 meshes. Thus, parallel computing becomes an essential requirement for recent CFD calculations where a number of processors are utilized at the same time.

2.1 Domain Decomposition for Multiple Processors

Different parallel computing methods can be applied depending on whether multiple processors share a single memory or use physically distributed memories. A parallel program in a shared memory system is relatively easy to implement using OpenMP library, since the calculation domain needs not to be decomposed for each processor. However, shared memory parallel computing is not efficient for a large scale calculation where cluster computers are often used with multiple memories and processors. Thus, the domain decomposition parallel computing on a distributed memory system is usually applied for large scale calculations.

In the domain decomposition method, the computational domain is divided as N subdomains for N processors after the mesh generation. For this, a manual partitioning is used for structured mesh, and the METIS library [15] is used for unstructured mesh. The number of computational cells in each subdomain is kept almost the same to satisfy the load balance for all processors. Each decomposed subdomain consists of internal cell, internal interface and external interface cells, as illustrated in Fig. 1. After the domain decomposition, the cells of each subdomain are renumbered in the order of internal cells, internal interface cells, and external interface cells. In each processor, only local values belonging to each subdomain are computed and stored. Since the data defined at the external interface cell belongs to another processor and memory, data communication is needed when the external interface

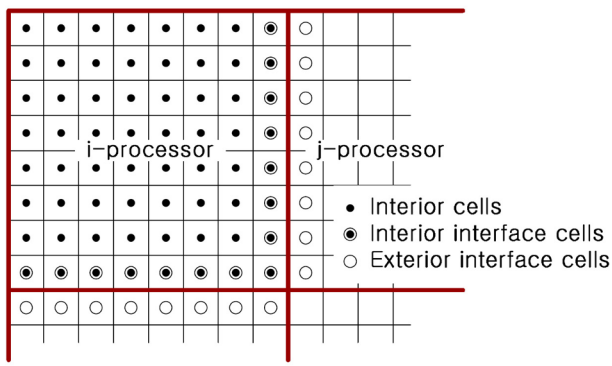

Fig. 1. Classification of Cells in a Subdomain

data is referenced in the calculation of a subdomain. This data communication among multiple processors during the calculation is allowed using the MPI (Message Passing Interface) library. Since the hardware in this study consists of the InfiniBand switch network, the MVAPICH2 library is adopted, which is known to show the best performance on the cluster machine with this network.

Most of the data communication appears in the calculation of the pressure matrix, where the CG (Conjugate Gradient) and Bi-CGSTAB (Bi-Conjugate Gradient STABlized) solvers are applied when the matrix is symmetric and asymmetric, respectively. The local matrix $[A_i]$ solving values at internal cells and internal interface cells in decomposed i-th subdomain can be typically constructed as follows:

$$[A_i]\{x_i\} = \{f_i\}$$

$$[A_i] = \begin{pmatrix} B_i & E_i & 0 \\ F_i & C_i & I_i^j \end{pmatrix}, \quad \{x_i\} = \begin{pmatrix} u_i \\ v_i \\ w_i^j \end{pmatrix}, \quad \{f_i\} = \begin{pmatrix} s_i \\ t_i \end{pmatrix}, \tag{1}$$

where $\{u_i\}$, and $\{s_i\}$ show the components from internal cells, $\{v_i\}$ and $\{t_i\}$ from internal interface cells, and $\{w_i^j\}$ from external interface cells. The superscript j indicates that i-th subdomain is linked with j-th subdomain. At each iteration step of the CG or BiCGSTAB solver, i-th subdomain sends $\{v_i\}$ to j-th subdomain and receives $\{w_i^j\}$ from the j-th subdomain to complete the matrix vector multiplication operation. All matrices are preconditioned with a block ILU (Incomplete Lower and Upper) decomposition parallel pre-conditioner [16]. The block ILU parallel pre-conditioner is applied to all subdomains with the following square block matrix:

$$\left[\tilde{A}_i\right] = \begin{pmatrix} B_i & E_i \\ F_i & C_i \end{pmatrix} \tag{2}$$

2.2 Efficiency of the Parallelized Code

The performance of the parallelized CUPID code, especially that of the pressure matrix solver, is evaluated by solving conceptual problems for both single- and two-phase fluid flow in a simple geometry. Figure 2 shows a three-dimensional rectangular channel of 0.1m × 0.1m × 4.0m where inlet flow and outlet pressure boundary conditions are given to the bottom and the top of the channel, respectively. The four side faces are wall boundaries. The outlet pressure is kept constant at 1 MPa. The inlet liquid is subcooled at 170 °C and flows into the channel with a velocity of 0.1m/s. For the two-phase flow calculation, a volumetric heat source of 23 MW/m^3 is given to the liquid column uniformly to generate a vapor phase. The simulation times are 20 seconds for both single- and two-phase flow calculations.

The overall runtime of the CUPID code, as well as the specific runtime of major routines, are investigated.

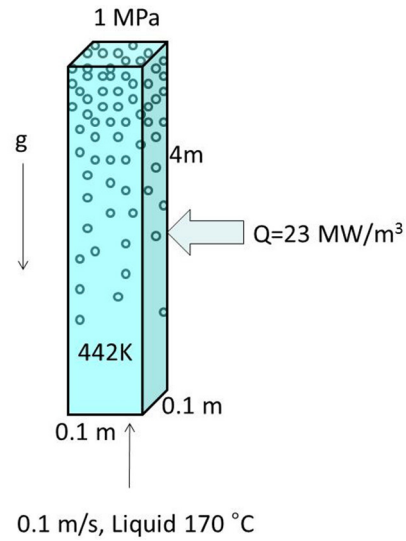

Fig. 2. Conceptual Problem for Parallel Performance Test

Two different numbers of 40,000 and 320,000 meshes are taken into account to evaluate the performance. The most time consuming routine is the calculation of the pressure matrix, where CG or BiCGSTAB solvers are applied as mentioned above. Table 1 summarizes the overall runtime for the coarse and fine meshes which include single- and two-phase calculations. The number of processors used in the calculation varied from 1 to 50, and the calculation domain has been partitioned as the corresponding number of processors.

The parallel performance is often indicated as scalability (η) defined as:

$$\eta = \frac{t_1}{t_p}, \tag{3}$$

where t_1 is the time for a serial calculation and t_p is the time for a parallel calculation using p processors. The results in Table 1 are shown in Fig. 3 for coarse and fine meshes, respectively, in terms of scalability. For the coarse mesh, the parallel performance with fewer than 4 processors shows linear scalability. Maximum speedup is expected to be about 20 times faster than a serial execution with 40 processors. It is because the communication time between processors is more dominant than an execution time within a subdomain. The fine mesh system improves the speedup ratio, as shown in Fig. 3. It is linearly scalable up to 20 processors for a single-phase flow test, and 16 processors for a two-phase flow test. The two-phase flow simulation is less scalable because its pressure matrix becomes asymmetric and the iteration number of the matrix solver increases, which results in more communication between the processors. The maximum speedup is 40 and 38 for single and two-phase flow tests with 50 processors.

Table 1. Overall Runtime of the Parallel test

Number of Cores	40,960 cells		320,000 cells	
	Single-phase (s)	Two-phase (s)	Single-phase (s)	Two-phase (s)
1	409	13404	14346	285509
3	215	6790	7310	148993
4	106	3271	3283	71245
8	57	1735	1909	41987
16	33	979	922	21837
20	29	876	880	20050
40	21	647	519	14150
50	22	672	438	13200

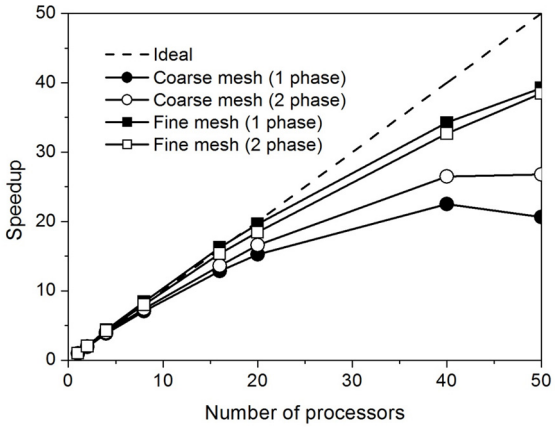

Fig. 3. Scalability of the Parallelized CUPID Code for Coarse and Fine Mesh

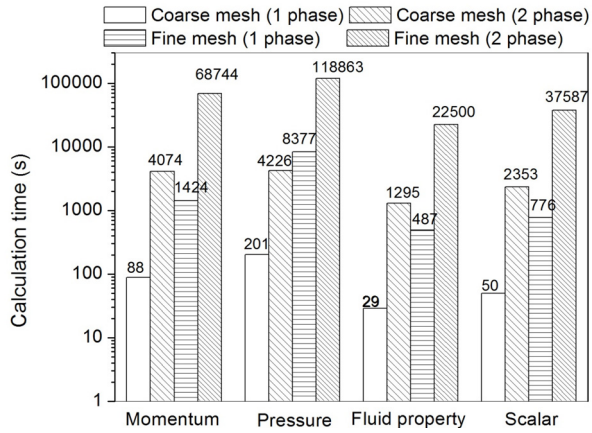

Fig. 4. Calculation Time of Major Routines

The parallel performance is also investigated for each major routine of the CUPID code. Since the CUPID code is based on a semi-implicit scheme, the overall runtime can be divided into four steps - explicit momentum, pressure, scalar, and fluid property calculations, where the pressure calculation is the most time consuming part. Figure 4 compares the specific runtimes of the four routines for single- and two-phase flow tests. The pressure routine takes a larger part in the overall runtime as the number of mesh increases. With the fine mesh, it is 81% of overall runtime for a single-phase flow test. It deceases to 53% for the two-phase flow test, since more calculations are expected for two-phase related variables. Figure 5 shows the scalability of each of the four routines for a two-phase flow test with the coarse mesh. The scalabilities of the three routines for explicit momentum, scalar, and fluid property calculations increase linearly with the number of processors, while the speedup of the pressure routine is lower than the others due to the data communication for solving the pressure matrix.

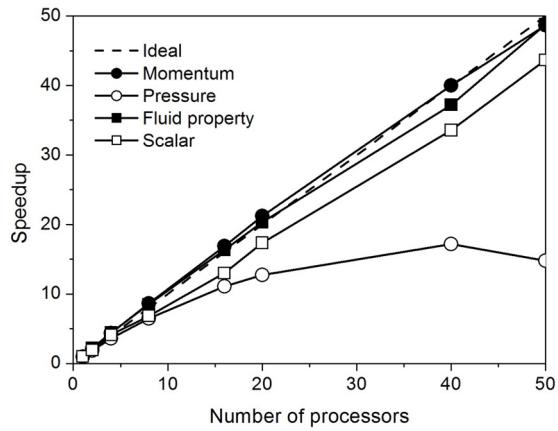

Fig. 5. Scalability of Each four Routines for Coarse Mesh

3. HEAT STRUCTURE COUPLING WITH THE MARS CODE

For a multi-scale thermal-hydraulic analysis of PWRs, the CUPID code has been coupled with a system-scale

thermal hydraulic code, MARS. In the coupled CUPID-MARS code, the coupling was achieved in two different ways, "flow field coupling" and "heat structure coupling". In the flow field coupling method, the pressure matrix of both codes were unified and solved at the same time. This is also called implicit coupling method and has an advantage in the transient two-phase flow simulation where the flow property at the coupled interface might change frequently [12]. On the other hand, in the heat structure coupling method, there is no fluid flow exchange at the interface; only heat transfers through. It is also called the explicit coupling method since the flow fields of both codes need not to be calculated simultaneously. Numerical instability does not appear in the explicit coupling method, since the temperature variation is much slower than the flow transient.

3.1 Coupling Method

The coupling interface between the two codes is the outer wall of the heat structure. The conduction equation for the solid interface is calculated by MARS. The two codes are coupled by sharing the heat structure surface temperatures at every time step by using the interactive control function of MARS. Then, designated pointer variables can be exchanged between MARS and CUPID when the latter calls the dynamic linked library (DLL) of the former. At first, the second outmost temperature of the heat structure (T_{solid}) was transferred from MARS to CUPID. With this solid temperature and the fluid temperature (T_{fluid}) at the closest fluid cell of CUPID to the wall, the wall temperature (T_{wall}) is determined from the heat transfer equation of CUPID. For sub-cooled boiling heat transfer, the following energy conservation equation [17] is solved to obtain T_{wall}:

$$
\begin{aligned}
q_{conduction} &= \frac{k_s(T_{solid}-T_{wall})}{r_{out}\cdot\ln(r_{out}/r_{in})} = q_{conv}+q_{quench}+q_{evap} \\
q_{conv} &= h_c A_{1f}\left(T_{wall}-T_{fluid}\right), \\
q_{quench} &= \left(\frac{2}{\sqrt{\pi}}\sqrt{t_w k_l \rho_l C_{pl} f}\right) A_{2f}\left(T_{wall}-T_{fluid}\right), \\
q_{evap} &= N'' f\left(\frac{\pi}{6}D^3_{b,depart}\right)\rho_g h_{fg}\,.
\end{aligned}
\tag{4}
$$

This heat partitioning model is employed in order to simulate the subcooled boiling. After that, the calculated wall temperature is transferred to MARS for the boundary condition of the heat conduction equation. MARS solves the conduction equation together with the convective boundary condition imposed on the inner tube wall, and the temperature distribution through the tube is obtained. Thereafter, the second outmost temperature is delivered again to CUPID for a new time step calculation. This procedure is repeated in all the fluid cells of CUPID, which include the heat structure for every time step.

3.2 Multi-scale Simulation of the Pool Mixing Test using the CUPID-MARS Code

The passive auxiliary feedwater system (PAFS) of APR+ is capable of condensing steam generated in a steam generator and re-feeding the condensed water to the steam generator by gravity [18]. The schematic of the PAFS is illustrated in Fig. 6. A pool mixing test facility was constructed for validating the cooling and operational performance of the PAFS. A single, nearly-horizontal U-tube, the dimension of which was the same as the prototypic U-tube of the PAFS, was simulated in the pool mixing test. Fulfilment of the heat removal requirement via the PAFS has been validated, and the major thermal-hydraulic parameters, such as local/overall heat transfer coefficients, fluid temperature inside the tube, wall temperature of the tube, and pool temperature distribution in the PCCT, were measured [18]. In the present study, the heat structure coupled CUPID-MARS code is applied to the analysis of the pool mixing test.

Figure 7 shows the 1D and 2D calculation meshes of the coupled CUPID-MARS code for the simulation of the pool mixing test loop. The PCHX tube is modelled with 40 sub-nodes of MARS. The slab geometry of the PCCT is modelled in two dimensions by assuming the depth directional flow behaviours are negligible. The effect of the two planes confining the slab is considered by implementing wall friction terms in the momentum equations of CUPID. A total of 1815 (33×55) meshes are used for the simulation described here [9].

Initially, the bottom half of the steam generator and the return-water line are filled with water, and the top half, the steam supply line, and the PCHX with steam. The initial pressure and water temperature in the primary side are 1.0 MPa and 40ºC, respectively. The PCCT water level is 9.8 m and the water temperature is 40ºC. At the right top of the PCCT, a constant atmospheric pressure boundary condition is given for the flow outlet.

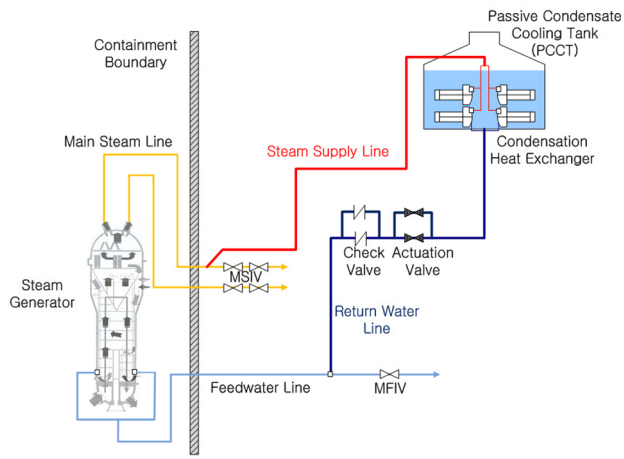

Fig. 6. Schematic Diagram of APR+ PAFS [18]

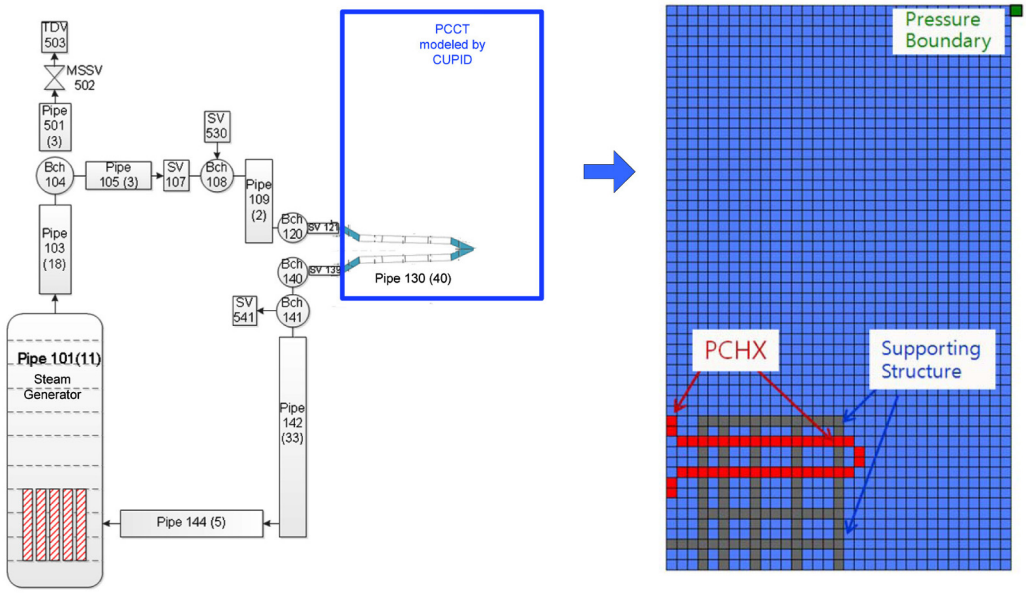

Fig. 7. 1D (MARS) and 2D (CUPID) Meshes for the Pool Mixing Test Loop

Figure 8 shows the calculated void fractions inside (MARS) and outside (CUPID) the PCHX, the wall vapour generation rate, and the liquid temperature distribution at 1200 seconds. The pure steam from the steam generator condenses as it flows through the PCHX and, at the outlet of the tube, the calculated void fraction is 0.86. Then the condensed water returns to the steam generator by gravity. In the PCCT, a subcooled boiling occurs on the PCHX, due to the condensation heat transfer from steam as shown in Fig. 8(c). The generated vapour immediately condenses, since the surrounding water is still subcooled, and thus the void fraction in the PCCT remains close to zero as indicated in Fig. 8(b). The liquid temperature outside the PCHX tube increases due to the boiling heat transfer, and a single-phase natural circulation starts, as shown in Fig. 8(d).

The single-phase natural circulation continues until 7000 seconds from the initiation of the transient. After that point, a two-phase region appears at the left side of the free surface, as presented in Fig. 9. It must be noted that this phase change was induced by the flashing of the super-heated water, whose temperature is 107°C, but was still subcooled at the elevation of the PCHX due to the hydraulic head. As the heated water reaches the free surface, the pressure decreases to atmospheric pressure, and vaporization occurs since now the liquid is above the saturation temperature.

After the flashing, the water temperature dropped to the saturation temperature and the liquid flows downward along the other side wall, and eventually, the two-phase natural circulation was established where the liquid is accelerated by bubbles, resulting in a remarkable increase of the liquid velocity. Due to the flashing near the free surface, the water level decreased gradually and reached the PCHX elevation at around 28800 seconds.

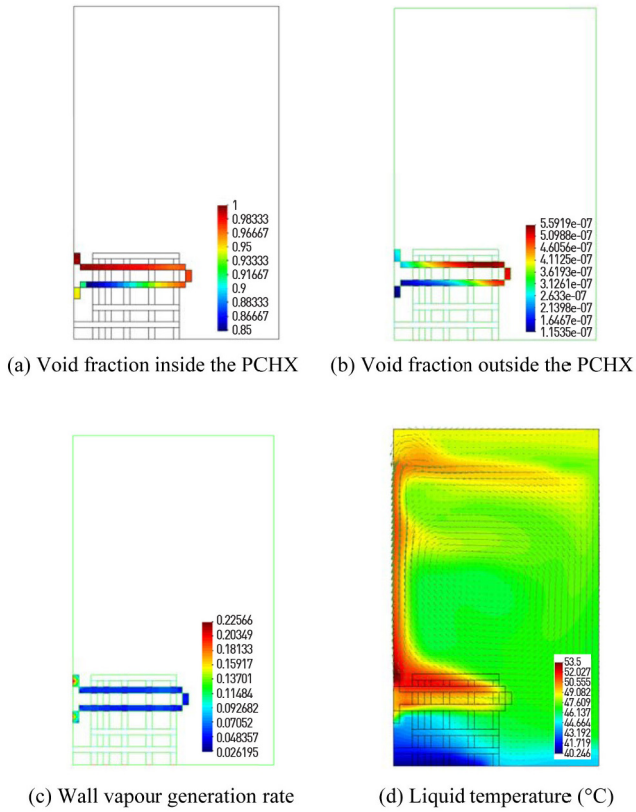

(a) Void fraction inside the PCHX (b) Void fraction outside the PCHX

(c) Wall vapour generation rate (d) Liquid temperature (°C)

Fig. 8. Calculation Results at t=1200 sec.

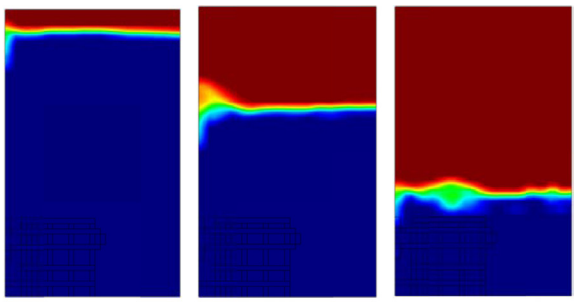

(a) 7000 sec. (b) 18000 sec. (c) 28800 sec.

Fig. 9. Water Level Decrease Due to the Boil-off

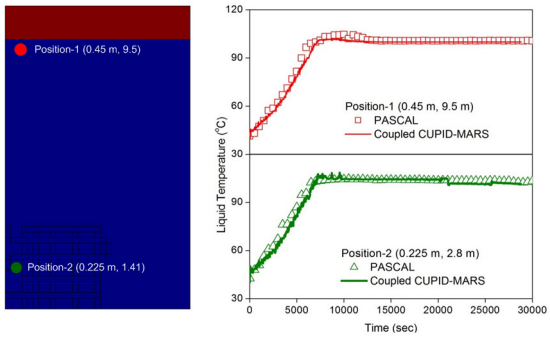

Fig. 10. Liquid Temperatures Transient

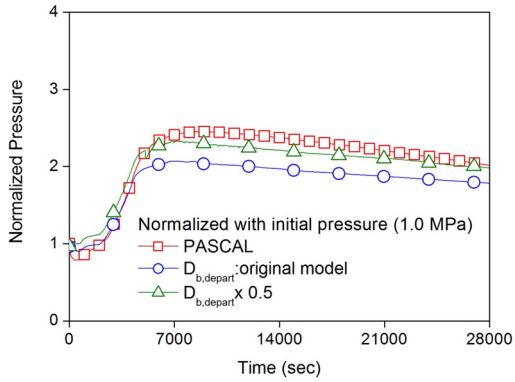

Fig. 11. Primary Side Pressure Transient

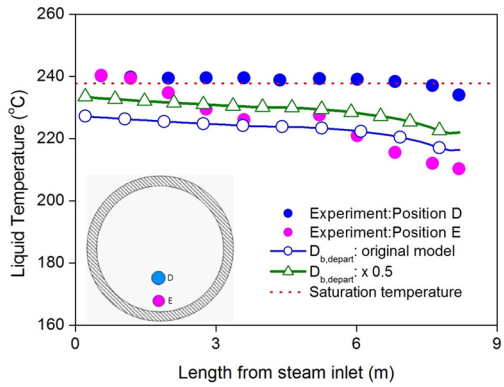

Fig. 12. Liquid Temperature Inside the PCHX Along the Tube Length

The liquid temperature transients at two different positions in the PCCT pool are compared with the experiment in Fig. 10; one is located 0.3 m below the initial free surface elevation (position-1) and the other 0.1 m below the PCHX steam inlet (position-2). The liquid temperature gradually increased from 40ºC with the heat release from the PCHX, and settled down as it reached the saturation temperature.

Figure 11 plots the primary side pressure transient at the inlet of the PCHX. The system pressure increased gradually with the increasing steam generator power for the early stage of the calculation before 5,000 seconds, which is well captured by the coupled code. However, after that, the calculation under-predicts the system pressure, although the decreasing trend of the pressure after 7000 seconds is well predicted. This difference is caused by the over-estimated boiling heat transfer coefficient of the heat partitioning model employed in the CUPID code. The predicted boiling heat transfer rate was found to vary significantly with the bubble departure diameter model and active nucleation site density model. For example, the sensitivity analysis for the bubble departure diameter was performed, and its reduction by half increased the system pressure in comparison to the experimental result, as shown in Fig. 11.

The liquid temperatures inside the PCHX at t=13,200 seconds are compared between the experiment and the calculation, in Fig. 12. As indicated in the figure, the temperature at the bottom thermocouple (position E) is lower than the saturation temperature, while the temperature at the second from the bottom (position D) is slightly higher than the saturation temperature in most of the region. This means that the condensed water level exists between two thermocouples and it is reasonable to assume that the averaged liquid temperature falls between the two measured temperatures. The comparison result shows that the present calculation under-predicts the liquid temperature because of the over-estimated boiling heat transfer coefficient as discussed above. The predicted liquid temperature is closer to the experiment data, with the modified bubble departure diameter used in the previous sensitivity analysis for the primary pressure.

The long transient of the pool mixing test has been successfully simulated using the CUPID-MARS code, and the important thermal-hydraulic issues related to the PAFS have been well resolved. This shows that the multi-scale thermal-hydraulic analysis using CUPID-MARS is very useful for the safety assessment of LWRs, which requires different spacial resolutions. Furthermore, the heat structure coupling method is easy to extend to other applications.

4. CUPID-SG FOR A STEAM GENERATOR THERMAL-HYDRAULIC ANALYSIS

CUPID-SG is a derivative of CUPID for exclusive use in analyzing thermal-hydraulics in PWR steam generators. To treat complex two-phase flow phenomena on the shell side of a steam generator, a set of constitutive models have been implemented, such as interfacial heat and mass transfer, interfacial drag, wall friction, and wall heat transfer models for tube bundle geometry. CUPID-SG supports unstructured meshes to treat the complex geometry of the steam generators. In this section, the physical models of CUPID-SG are summarized, and the FRIGG bundle test [19] is assessed for the validation of the code.

4.1 Porous Media Models for Tube Bundles

A porous media approach is applied to a component-scale analysis of a steam generator packed with tube bundles. Complex configurations of internal structures are simplified by porosities and permeabilities for cell volumes and faces. Heat conductors are evenly distributed in a cell with a given porosity when heating surfaces exist in a porous media. The constitutive models for interfacial transfer depend on a flow regime map. CUPID-SG uses the vertical flow regime map of MARS and only the unstratified pre-CHF regime map is implemented, as shown in Fig. 13, since CUPID-SG is intended to be used for performance analysis during the normal operation of a PWR steam generator.

The transition between bubbly and slug flow occurs when

$$\alpha_{BS}=\begin{cases}\alpha_{BS}^{*} & G_m \le 2000\ \mathrm{kg/m^2s},\\ \alpha_{BS}^{*}+\dfrac{\left(0.5-\alpha_{BS}^{*}\right)}{1000}\left(G_m-2000\right) & 2000<G_m<3000\ \mathrm{kg/m^2s},\\ 0.5 & G_m \ge 3000\ \mathrm{kg/m^2s}.\end{cases} \quad (5)$$

where

$$\alpha_{BS}^{*}=\max\left[0.25\min\left\{1,\left(0.045D^{*}\right)^{8}\right\},10^{-3}\right],$$

$$D^{*}=D\left[\frac{g\left(\rho_f-\rho_g\right)}{\sigma}\right]^{1/2}\ge 19.11.$$

The lower boundary of the annular-mist flow regime is

$$\alpha_{SA}=\max\left[\alpha_{AM}^{min},\min\left\{\alpha_{crit}^{f},\alpha_{crit}^{e},\alpha_{BS}^{max}\right\}\right] \quad (6)$$

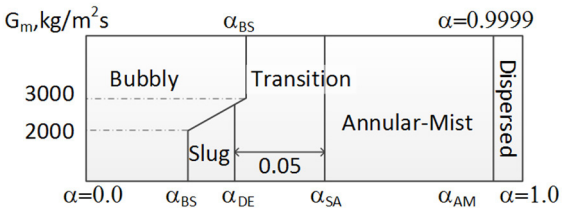

Fig. 13. Flow Regime Map of CUPID-SG

where

$$\alpha_{AM}^{min}=0.5,\quad \alpha_{BS}^{max}=0.9,\quad \alpha_{crit}^{e}=\frac{3.2}{V_g}\left[\frac{g\sigma\left(\rho_f-\rho_g\right)}{\rho_g^2}\right]^{1/4},$$

$$\alpha_{crit}^{f}=\begin{cases}\dfrac{1}{V_g}\left[\dfrac{g\sigma\left(\rho_f-\rho_g\right)}{\rho_g^2}\right]^{1/2} & \text{for upflow},\\ 0.75 & \text{otherwise}.\end{cases}$$

The slug flow begins to turn into the annular-mist flow at

$$\alpha_{DE}=\max\left[\alpha_{BS},\alpha_{SA}-0.05\right] \quad (7)$$

The interfacial area is dependent on the flow regime map. Small bubbles appear in a bubbly flow and in a slug flow. The interfacial area concentration of small bubbles is

$$a_{SB}=\frac{3.6\alpha_{SB}}{D_b} \quad (8)$$

where $D_b(=We_{crit}\sigma/\rho_l v_{fg}^2)$ is the average bubble diameter. The critical Weber number is 5 for small bubbles. The interfacial area concentration of Taylor bubbles (TBs) in a slug flow is

$$a_{TB}=\frac{4.5}{D}\alpha_{TB}\times\left(2.0\right) \quad (9)$$

where 2.0 is a roughness factor. The volume fraction of Taylor bubbles is defined as

$$\alpha_{TB}=\frac{\alpha-\alpha_{gs}}{1.0-\alpha_{gs}} \quad (10)$$

where the average void fraction, α_{gs}, in liquid film and slug is calculated as

$$\alpha_{gs}=\alpha_{BS}\exp\left(-8\frac{\alpha-\alpha_{BS}}{\alpha_{SA}-\alpha_{BS}}\right) \quad (11)$$

The interfacial area concentration in an annular-mist flow is

$$a_{ANN}=\frac{4}{D}\left(1-\alpha_{ff}\right)^{1/2}\times 2.5\left(30\alpha_{ff}\right)^{1/8} \quad (12)$$

where 2.5 is a roughness factor and α_{ff} is the average volume fraction of the liquid film. At present, CUPID-SG assumes there are no droplets in the core vapor region of an annular-mist flow. The interfacial area concentration in the transition region is linearly interpolated by a vapor fraction with the interfacial area concentration of bubbles and a liquid film.

Interfacial heat transfer, interfacial momentum transfer, wall friction and wall heat transfer models used in CUPID-SG are summarized in Table 2.

4.2 Analysis of FRIGG Test

CUPID-SG is validated against the FRIGG experiment [19]. The test cases which were used in validating the ATHOS3 code are chosen for this benchmark. The selected cases are simulated with CUPID-SG and the results by

Table 2. Physical Models of CUPID-SG

Interfacial heat transfer [20]	Bubble flow	Slug flow	Annular flow	Churn flow
	Pessset-Zwick, Lee-Ryley correlation	Unal and Lahey, Lee-Ryley correlation	Theofanous, Dittus-Boelter correlation	Interpolated from the values at the regime boundaries (α_{DE} , α_{BS} , and α_{SA})
Interfacial momentum transfer [20]	Small and Taylor bubble		Annular-mist flow	
	Ishii and Chawla correlation		$F_{il,ANN} = \frac{1}{2}\rho_l \lvert v_R \rvert v_R f_{i,ANN} a_{i,ANN}$ $f_{i,ANN}$: obtained depending on the flow conditions - laminar or turbulent, co-current, counter-current, horizontal, vertical	
Wall friction	Axial flow		Cross flow [21, 22]	
	$F_z = f_a A_{SV} \rho \lvert v_z \rvert v_z \Phi$ f_a : friction factor for axial flows A_{SV} : wetted surface area / m^3 v_z : axial velocity Φ : two-phase multiplier,		$F_x = f_c C_A C_V A_{SV} \rho \lvert v_x \rvert v_x \Phi$ $F_y = f_c C_A C_V A_{SV} \rho \lvert v_y \rvert v_y \Phi$ $f_c = \frac{0.432}{Re^{0.205}}, C_A = \frac{4\beta_V P_V \sin\theta}{\pi d_e}, C_V = \left(\frac{\beta_V P_V}{P_V - D}\right)^2$ β_V : porosity, d_e : equivalent hydraulic diameter P_V : pitch, D : tube diameter	
Wall heat transfer [20]	Single phase		Two-phase	
	Forced convection	Dittus-Boeter correlation	Boiling heat transfer	Chen correlation
	Natural convection	Churchil-Chu or McAdams correlation	Subcooled nucleate boiling	Saha and Zuber correlation

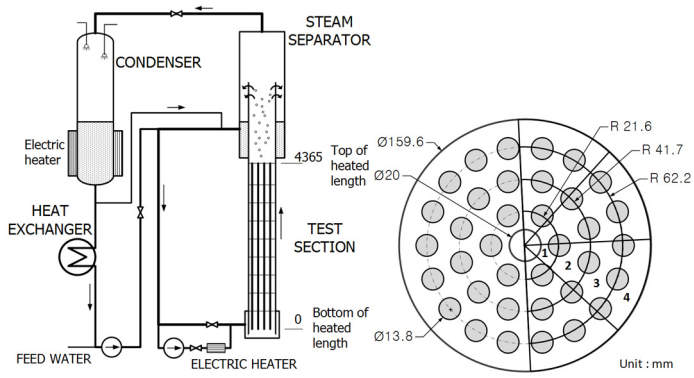

Fig. 14. Schematics of FRIGG Test and Rod Layout (units in mm) [19]

CUPID-SG are compared with those of ATHOS3 and the measured data.

Figure 14 shows a schematic of the FRIGG test facility. The test section has 36 heater rods and a support rod at the center. The heater rods are distributed along the circumference of three concentric circles. Subcooled water flows into the test section at the bottom in the radial direction. The flow bends upward and escapes the test section in the vertical direction at the top. The axial and radial distributions of the void fraction were measured

Table 3. FRIGG Test Cases

FRIGG Test No.	Description	Pressure	Subcooling	Heat Flux	Mass Flux	Exit Quality
		MPa	°C	kW/m²	kg/m²s	-
613118	**Baseline**	**5.00**	**26.6**	**663**	**1018**	**0.111**
613010	High exit quality	4.87	2.0	815	497	0.468
613123	Low pressure	3.02	5.7	660	2011	0.073
613130	High pressure	6.88	6.6	663	1995	0.081

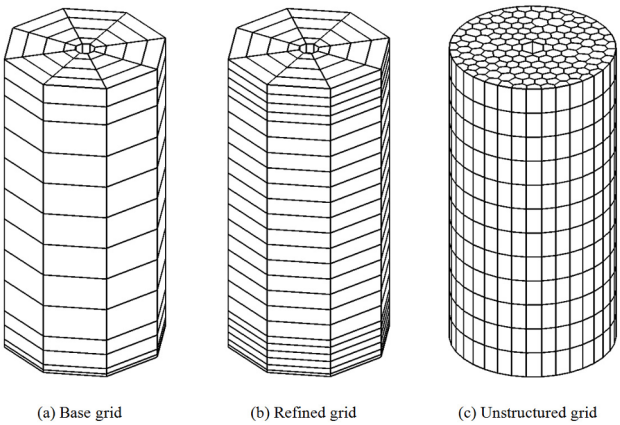

(a) Base grid (b) Refined grid (c) Unstructured grid

Fig. 15. Grids for CUPID-SG Validation (Not in Scale)

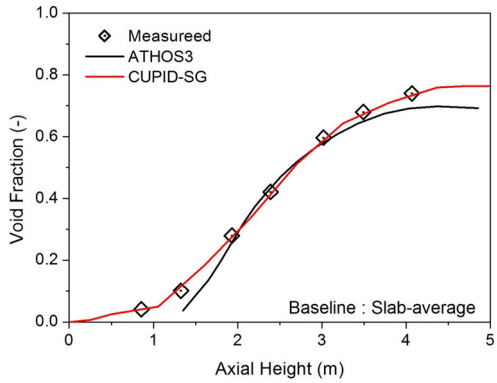

Fig. 16. Slab-averaged Void Fraction (Baseline with the Base Grid)

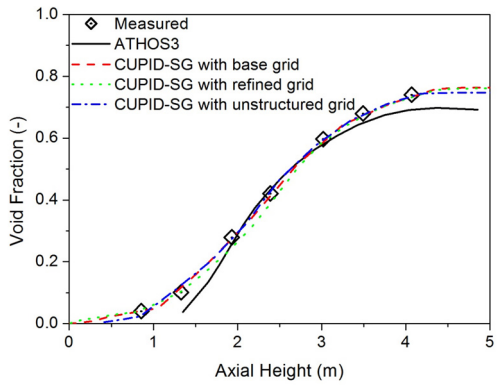

Fig. 17. Void Fraction with the Base, Refined and Unstructured Grids

and the axial distributions of slab-averaged void fraction and void fractions in the four radial zones were presented in the experiment results. ATHOS3 had been validated against four steady-state test cases with varying thermal-hydraulic conditions. Table 3 shows the test conditions of the four validation cases.

Figure 15 shows the computational mesh for benchmarking calculations of CUPID-SG. Hexahedron cells are used to build the structured grids in Figs. 15(a) and 15(b). The cross-section of the structured grids is divided into eight sections in the circumferential direction, as done for the ATHOS3 validation. The top face of the domain is set as a pressure boundary. The velocity boundary is the outer-most lateral faces at the lowest level. Figure 15(c) is a computational grid with polygonal prism cells. This unstructured grid has better resolution in the outer region than the structural grids.

Figure 16 is the slab-averaged void fraction along the axial position for the baseline case. For the baseline case, subcooled water is injected in a radial direction at the bottom of the test section with a mass flux of 1018 kg/m²s. The water is subcooled to 26.6ºC. The system pressure is 5 MPa and the average heat flux is 663 kW/m². CUPID-SG predicts the void fraction more closely to the measurements than ATHOS3, especially at the lower subcooled region and the upper high voidage region. CUPID-SG has a heat partition model to describe the vapor buildup in subcooled regions, while ATHOS3 cannot predict the existence of vapor in subcooled regions.

Figure 17 shows the calculation results with the base grid, refined grid and unstructured polygonal grid shown in Fig. 15. The result shows that CUPID-SG makes a good prediction on the void fraction near the inlet where a multi-dimensional effect exists and subcooled boiling occurs. Little difference is observed in the results with

the base and refined grids. The result indicates that the base grid in Fig.17 has a sufficient axial resolution. The mesh results in an even better prediction of the void fraction than the structured meshes, as shown in Figs. 15(a) and 15(b). The unstructured mesh enables even distribution of cell sizes over the cross-section and reduces geometric distortion of the structured meshes with a finite number of circumferential sections. The result verifies that the newly introduced models for steam generator simulation work well with the unstructured meshes supported by CUPID-SG.

5. CONCLUSIONS

KAERI has been developing the CUPID code for analyzing transient two-phase flows in LWRs in a component- or CFD-scale. For more practical use of CUPID as a multi-scale thermal-hydraulic analysis code, new features have been implemented which include parallelization, heat structure coupling with MARS and the development of a new version for steam generator analysis.

For the parallelization of CUPID, a domain decomposition method has been applied. The code structure has been modified to decompose the computation domain, and redefine the global variables for each processor. The MPI library has been used for data communication among the processors. A parallel performance test showed that the scalability is linearly proportional to the number of processors for the calculation routines of explicit momentum, scalar, and fluid property where data communication is small. For the pressure calculation routine, the scalability was saturated with an increasing number of processors due to significant data communication.

The CUPID code has been coupled with MARS for a multi-scale thermal-hydraulic analysis. The coupling was achieved using the heat structure of MARS where fluid flow exchange does not occur. Eight hours of a long term transient of the pool mixing test loop was successfully simulated using CUPID-MARS, where the steam supply system including PCHX is calculated by MARS, and the thermal mixing in the PCCT is simulated by CUPID. This is one of the practical applications of a multi-scale thermal-hydraulic analysis.

CUPID-SG is being developed to analyze the thermal-hydraulic performance of PWR steam generators. In comparison with an existing steam generator code, CUPID-SG has advantages that it can deal with the complex geometries of unstructured meshes, has constitutive models to describe wider spectrum of boiling heat transfer, and is arranged on the basis of a modern two-fluid model. CUPID-SG is validated by comparing the prediction on the FRIGG experiment, which is one of the validation problems of ATHOS3, with the measured data for both structured and unstructured meshes. The benchmark confirms that CUPID-SG integrated with the constitutive models can appropriately analyze boiling flows over tube bundles, which is typical in PWR steam generators.

With these newly implemented features, the CUPID code is able to assess a wide range of thermal-hydraulic safety issues of LWRs with the relevant space resolutions of CFD-, component- and system-scale.

ACKNOWLEDGMENTS

This work was supported by the National Research Foundation of Korea (NRF) and the Korea Radiation Safety Foundation (KORSAFe) grant funded by the Korean government (MSIP & NSSC) (Nuclear Research and Development Program: 2012M2A8A4025647, Nuclear Safety Research Center Program: 1305011).

NOMENCLATURE

A	Area
C_p	Specific heat
D	Diameter
f	Bubble departure frequency
h	Heat transfer coefficient or Enthalpy
k	Conductivity
LWR	Light Water Reactor
N''	Active nucleation site density
PWR	Pressurized Water Reactor
q	Heat transfer rate
r	Radius
t	Time
T	Temperature
v	Specific volume
We	Weber number

Greek Letter

α	Void fraction
η	Scalability
ρ	Density
σ	Surface tension

Subscripts

ANN	Annular
b	Bubble
c	Convection
$crit$	Critical
fg	Difference between liquid and gas
g	Gas
l	Liquid
SB	Small bubble
TB	Taylor bubble
w	Waiting
$1f$	Single phase
$2f$	Two phase

REFERENCES

[1] J. J. Jeong, K. S. Ha, B. D. Chung, and W. J. Lee, "Development of a multi-dimensional thermal-hydraulic system code, MARS 1.3.1," *Annals of Nuclear Energy*, vol. 26, no. 18, pp. 1611-1642 (1999).

[2] D. R. Lilies and W. H. Reed, "A semi-implicit method

for two-phase fluid dynamics," *Journal of Computational Physics*, vol. 26, pp. 390-407 (1978).
[3] M. Robert, M. Farvacque, M. Parent, and B. Faydide, "CATHARE 2 V2.5: A Fully Validated CATHARE, Version for Various Applications," *Proc. 10th Int. Topl. Mtg. Nuclear Reactor Thermal Hydraulics (NURETH 10)*, Seoul, Republic of Korea, October 5–9, 2003.
[4] P. Coste, J. Lavieville, J. Pouvreau, C. Baudry, M. Guingo, and A. Douce, "Validation of the Large Interface Model of NEPTUNE_CFD 1.0.8 for Pressurized Thermal Shock (PTS) applications," *Nuclear Engineering and Design*, vol. 253, pp. 296-310 (2012).
[5] J. J. Jeong, H. Y. Yoon, I. K. Park, and H. K. Cho, "The CUPID Code Development and Assessment Strategy," *Nuclear Engineering and Technology*, vol. 42, no. 6, pp. 636-655 (2010).
[6] H. Y. Yoon, H. K. Cho, J. R. Lee, I. K. Park, and J. J. Jeong, "Multi-scale thermal-hydraulic analysis of PWRs using the CUPID code," *Nuclear Engineering and Technology*, vol. 44, no. 8, pp. 831-846 (2012).
[7] L. S. Caretto, A. D. Gosman, S. V. Patankar, D. B. Spladding, "Two calculation procedures for steady, three-dimensional flows with recirculation," *Proc. 3rd Int. Conf. Numerical Methods in Fluid Dynamics*, Paris, France 1972.
[8] H. Y. Yoon, J. J. Jeong, H. K. Cho, Y. S. Bang, K. W. Seul, "A Multi-scale analysis of the transient behavior of an advanced safety injection Tank," *Annals of Nuclear Energy*, vol. 62, pp. 17-25 (2013).
[9] H. K. Cho, S. J. Lee, H. Y. Yoon, K.-H. Kang, and J. J. Jeong, "Simulation of single- and two-phase natural circulation in the passive condensate cooling tank using the CUPID code," *Journal of Nuclear Science and Technology*, vol. 50, no. 7, pp. 709-722 (2013).
[10] OpenMP Architecture Review Board, *OpenMP Application Program Interface, version3.1* (2011).
[11] M. Snir, S. Otto, S. Huss-Lederman, D. Walker, and J. Dongarra, *MPI: The Complete Reference*, the MIT Press (1996).
[12] I. K. Park, J. R. Lee, S. W. Lee, H. Y. Yoon, and J. J. Jeong, "An implicit code coupling of 1-D system code and 3-D in-house CFD code for multi-scaled simulations of nuclear reactor transients," *Annals of Nuclear Energy*, vol. 59, pp. 80-91 (2013).
[13] K.-H. Kang, S. Kim, B.-U. Bae, Y.-J. Cho, Y.-S. Park, B.-J. Yun, "Separate and integral effect tests for validation of cooling and operational performance of the APR+ passive auxiliary feedwater system," *Nuclear Engineering and Technology*, vol. 44, no. 6, pp. 597-610 (2012).
[14] L. W. Keeton, A. K. Singhal, and G. S. Srikantiah, "ATHOS3 Mod-01: A computer program for thermal-hydraulic analysis of steam generator, volume 1: Mathematical and physical models and method of solution (revision 1)," Technical Report NP-4604-CCML, EPRI (1990).
[15] G. Karypis and V. Kumar, "Multilevel k-way Partitioning Scheme for Irregular Graphs," *J. Parallel Distrib. Comput*. vol. 48, no. 1, pp. 96-129 (1998).
[16] A. Gupta, V. Kumar and A. Sameh, "Performance and scalability of preconditioned conjugate gradient methods on parallel computers", *IEEE Transactions on Parallel and Distributed System*, vol. 6, no. 5, pp. 455-469 (1995).
[17] N. Kurul, M. Z. Podowski, "On the modeling of multidimensional effects in boiling channels," *ANS Proceedings of 27th National Heat Transfer Conference*, Minneapolis, MN, USA, 1991.
[18] S. Kim, B.-U. Bae, Y.-J. Cho, Y.-S. Park, K.-H. Kang, B.-J. Yun, "2013. An experimental study on the validation of cooling capability for the passive auxiliary feedwater system (PAFS) condensation heat exchanger," *Nuclear Engineering and Design*, vol. 260, pp. 54-63 (2013).
[19] J. W. Heistand and J. G. Thakkar, "ATHOS and FLOW3 simulation of the FRIGG heated rod bundle experiment," Technical Report NP-3514, EPRI (1984).
[20] KAERI Thermal Hydraulic Safety Research Division, "MARS code manual volume V: Models and correlations," Technical Report KAERI/TR-3872/2009, KAERI (2009).
[21] W. H. Kays and A. L. London, "*Compact Heat Exchangers*", 2nd ed., McGraw Hill, New York (1964).
[22] E. D. Grimison, "Correlations and Utilization of New Data on Flow Resistance and Heat Transfer for Cross Flow of Gases over Tube Banks," *ASME Trans*., vol. 59, p. 583 (1937).